ISSN 1648-7788 / eISSN 1822-4180

VILNIUS TECH
Vilnius Gediminas Technical University

AVIATION

2026
Volume 30
Issue 1
Pages 24–32
https://doi.org/10.3846/aviation.2026.25922

IMPROVED METHOD FOR DETERMINING RHEOLOGICAL PARAMETERS OF COMPOSITE MATERIALS DURING CREEP UNDER TORSIONAL DEFORMATION

Bidzina ABESADZE [1]✉, Saba KOPALIANI [2]

[1]*Scientific-Research Centre, Georgian Aviation University, Tbilisi, Georgia*
[2]*Faculty of Engineering, Georgian Aviation University, Tbilisi, Georgia*

Article History:
- received 11 June 2025
- accepted 24 November 2025

Abstract. This paper presents an improved method for determining rheological function parameters of viscoelastic-plastic materials, demonstrated through creep under torsional deformation. The approach is based on the heredity theory (Boltzmann's principle), using curve fitting to identify parameters (A, α, and β). The improved method from previous studies uses precise graph construction via computational tools, with curve alignment performed using a least square–like approach. An extended database of theoretical rheological function graphs and tables, developed from complex mathematical models and prior research, was employed in the analysis. Importantly, the study highlights that modern aircraft structures, where a significant portion of elements are made of advanced composite materials, are exposed during flight to complex, time-dependent loading conditions. Under these conditions, creep phenomena may develop within structural components, leading to residual deformations and gradual degradation of mechanical properties over time. Even with initially high safety margins, such effects can eventually cause the failure of critical elements after prolonged operation. Therefore, the presented method provides a scientific and practical tool for assessing and predicting the long-term viscoelastic–plastic behavior of aviation composites, ensuring structural integrity, flight safety, and an extended operational lifetime of aircraft.

Keywords: aircraft, composite material, rheology, creep, influence function, torsional deformation.

✉Corresponding author. E-mail: *bidzina_abesadze@ssu.edu.ge*

1. Introduction

Materials with viscoelastic-plastic properties such as various types of plastics or composite materials based on them, exhibit complex deformation behavior under loading, manifested in their rheological characteristics. In the simplest case, this behavior is described through creep and relaxation processes (Dumbadze, 2015; Abesadze, 2019; Nijssen, 2015, Abesadze, 2020).

Within the framework of linear hereditary theory, the influence and relaxation functions are defined. These functions are used to characterize the rheological relationship between stress and strain. In its general form, the time-dependent strain is expressed as follows:

$$\varepsilon(t)=\frac{1}{E}\left[\sigma(t)+\int_0^t K(t-\tau)\sigma(\tau)d\tau\right]. \quad (1)$$

A relatively simpler case is the creep process**,** which involves describing the time-dependent deformation of a material under a constant applied stress, i.e., when the load is maintained at a constant value: $\sigma(t)=\sigma_c=const$. Under these conditions, Equation (1) simplifies to:

$$\varepsilon(t)=\frac{\sigma_c}{E}\left[1+\int_0^t K(t-\tau)d\tau\right], \quad (2)$$

where σ_c is the constant applied stress, E is the elastic modulus, and $K(t-\tau)$ is the influence function (Abesadze & Kopaliani, 2024; Abesadze & Kelikhashvili, 2023; Findley et al., 1976). Equation (2), the integral equation, can appear in several forms. In the present study, the representation defined by M. Koltunov (Dumbadze, 2015; Gibson, 2016; Amir, 2024; Barbero, 2018) is employed:

$$K(t-\tau)=\frac{e^{-\beta(t-\tau)}}{(t-\tau)}\sum_{n=1}^{n=\infty}\frac{\left[A\tilde{A}(\alpha)\right]^n(t-\tau)^{n\alpha}}{\tilde{A}(\alpha n)}. \quad (3)$$

Equation (3) contains three independent parameters A, α and β whose specific values determine the rheological functions for a given material.

For viscoelastic-plastic materials, creep behavior is also observed under torsional deformation (Lakes, 2009; Ward & Sweeney, 2012; Ferry, 2018). Consider a cylindrical tube-shaped body characterized by the following param-

eters: outer diameter D, inner diameter d, and height l. The body is fixed at one base, while a torsional moment M_z is applied to the opposite base (see Figure 1). Taking the creep process into account, the angle of rotation at the free end becomes a time-dependent function, $\varphi(t)$. The general form of the expressions and parameters describing torsional deformation remains analogous to those for isotropic bodies. In particular, the shear strain is given by:

$$\gamma(t) = R\frac{\varphi(t)}{l} = R\cdot\theta(t), \tag{4}$$

where

$$\theta(t) = \frac{d\varphi(t)}{dz} = \frac{\varphi(t)}{l} \tag{5}$$

intensity of the angle of twist.

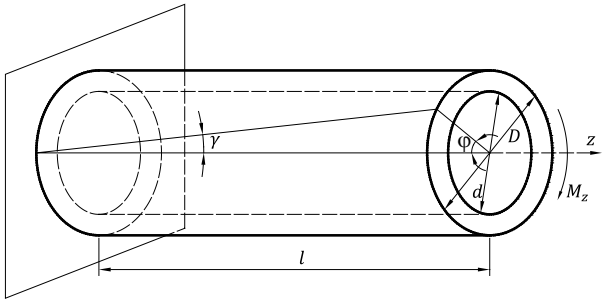

Figure 1. Scheme of torsion for the cylindrical tube specimen under investigation

Regarding the relationship between the torsional moment, stress, and angle of twist, the standard approach is applied analogously (Dumbadze, 2015):

$$\tau(t) = G\cdot\gamma(t) = G\cdot\rho\cdot\theta(t), \tag{6}$$

where G is the shear modulus of the material, and the torsional moment is defined:

$$M_z(t) = \int\tau(t)\rho dF = G\theta(t)\int\rho^2 dF = G\theta(t)I_P, \tag{7}$$

$I_P = \int\rho^2 dF$, the polar moment of inertia for the cross-section (Beer et al., 2015).

From Equation (6), the twist angle intensity can be represented as a time-dependent function tied to the torsional moment. Similarly, to Equation (1), it is written as:

$$\theta(t) = \frac{1}{GI_P}M_z(t) = \frac{1}{GI_P}\left[M_z(t) + \int_0^t K(t-\tau)M_z(\tau)d\tau\right], \tag{8}$$

$K(t-\tau)$, Creep is inherent to pure torsion. Assuming the torsional moment is constant, $M_z = const$, then Equation (7) takes the form:

$$\theta(t) = \frac{M_z}{GI_p}\left[1 + \int_0^t K(t-\tau)d\tau\right]. \tag{9}$$

Equations (2) and (8) include the term $\int_0^t K(t-\tau)d\tau$ a purely theoretical function. A reference dataset has been developed, containing families of theoretical curves and corresponding tables of function values for various combinations of the parameters (A, α and β) (Dumbadze, 2015). Despite the volume of data, the database remains incomplete. Modern computational tools and software enable substantial expansion of this resource.

Abesadze and Kopaliani (2024) provide a detailed description of the procedures for carrying out the required calculations in Maple, including a method based on transformation to the complex plane during integration. The present study adopts a similar approach.

2. Research methodology

2.1. General case of matching experimental and theoretical curves

In the course of this study, similarly to previous research (Abesadze & Kopaliani, 2024; Abesadze & Kelikhashvili, 2023), the experimental and theoretical data are aligned using an improved fitting method that ensures the best possible match between the corresponding curves. Typically, the alignment is performed on a logarithmic scale, where both curves are plotted using the same axis scaling. One of the curves is shifted horizontally and vertically to achieve the best overlap with the other. The parameters of this displacement provide additional insight into the characteristics of the analyzed process.

If the theoretical and experimental curves are defined analytically by the functions $f(t_{th})$ and $f(t_{exp})$, respectively, then their alignment on a logarithmic scale (see Figure 2) yields the following relationship:

$$\ln\left[f_{exp}(\ln t_{exp})\right] = \ln\left[f_{th}(\ln t_{th} + \ln k)\right] - \ln a = \ln\left(\frac{1}{a}\cdot f_{th}(\ln(k\cdot t_{th}))\right). \tag{10}$$

From Equation (9), the relationship between the theoretical and experimental functions becomes readily apparent.

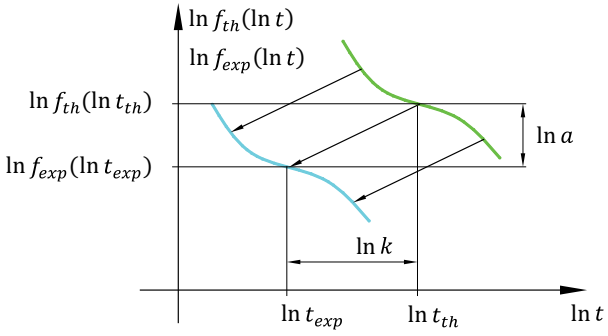

Figure 2. Alignment of theoretical and experimental curves on a logarithmic scale

$$f_{exp}\left(t_{exp}\right)=\frac{1}{a}\cdot f_{th}\left(\ln\left(k\cdot t_{th}\right)\right). \quad (11)$$

The parameters a and k can be directly determined from the graphs. Depending on the specific problem, the theoretical curve may be translated parallel to the coordinate axes, in accordance with the described relationships.

The essence of the improved approach to curve alignment lies in determining the fitting parameters a and k not visually from the graphs, but analytically, with high precision. This requires expressing both the theoretical and experimental functions analytically for the process under consideration. Although the theoretical function has a defined analytical form for instance, as given in Equation (8) its direct use in subsequent calculations is often inconvenient. Therefore, it is preferable to approximate the function by a polynomial $P_n\left(t\right)$ of degree n, whose coefficients are determined by solving a system of equations based on the condition that the polynomial matches the function at n + 1 preselected points (Abesadze & Kopaliani, 2024).

$$P_n\left(t_i\right)=f_{th}\left(t_i\right)\quad P_n\left(\ln t_i\right)=\ln f_{th}\left(\ln t_i\right)\quad i=1\cdots n+1. \quad (12)$$

To achieve the best possible match between the theoretical function and its corresponding polynomial, it is desirable to choose a high degree n, while ensuring that the points t_i lie outside the time interval specified by the problem under consideration. This is because, within the framework of the present study and for the specific example analyzed, the theoretical curve will undergo a smooth translation. The argument can therefore be shifted beyond the interval of interest without resorting to extrapolation or introducing significant deviation from accurate values.

As for the experimental curve, it should be constructed based on discrete experimental data points, which are subject to some degree of scatter due to measurement uncertainties. An averaged curve must be generated using the least squares method, approximated by a polynomial $P_m\left(t\right)$ of relatively low degree m. A lower polynomial degree m helps avoid local overfitting to the scattered experimental points. Since the experimental curve cannot be extended beyond the given time interval without extrapolation, all operations must be confined strictly to the interior of this interval. Therefore, during the curve-matching process, it is preferable to keep the experimental curve fixed (Draper & Smith, 1998).

Subsequently, for a predefined set of N points, the following expression should be constructed according to Equation (9):

$$S_N=\sum_{i=1}^{N}\left[P_n\left(\ln t_i-\ln k\right)-\ln a-P_m\left(\ln t_i\right)\right]^2\rightarrow\min. \quad (13)$$

In the case of a perfect match between the curves, Equation (7) would evidently be equal to zero. However, such ideal agreement is not attainable in practice. The proposed strategy is analogous to the method of least squares. To minimize the sum defined in Equation (7), the following condition must be satisfied:

$$\frac{\partial S_N}{\partial\left(\ln a\right)}=0\ \text{ and }\ \frac{\partial S_N}{\partial\left(\ln k\right)}=0. \quad (14)$$

As a result, a system of two equations with two unknowns is obtained. Solving this system allows for the unique determination of the parameters a and k. The solution can be found using numerical methods.

2.2. Polynomial approximation considerations

When fitting experimental rheological data with polynomials, the choice of polynomial degree plays a critical role in balancing fidelity and stability of the approximation. If the experimental points originate from an underlying smooth function with low measurement noise, employing a relatively high-degree polynomial can yield an accurate representation without introducing spurious oscillations or local extrema. In such cases, higher-order terms capture the intrinsic curvature of the true function while preserving its monotonic character (Epperson, 2013).

Conversely, when the data exhibit noticeable scatter, using a high-degree polynomial in a least-squares fit often leads to overfitting. The resulting curve may develop nonphysical local maxima, minima, or inflection points that do not reflect the material's actual rheological response. These artifacts sometimes referred to as Runge phenomena arise because the fitting process attempts to pass too closely through each noisy point. For experimental creep data with unavoidable measurement variability, it is therefore prudent to select a moderate or low polynomial degree or to employ regularization or smoothing techniques to suppress unwarranted oscillations while still capturing the overall trend.

In the context of torsional creep analysis, this distinction is essential. Theoretical curves, which are smooth by construction, can be safely approximated by higher-degree polynomials beyond the experimental time interval, enabling accurate analytical integration and transformation. Experimental curves, however, should generally be approximated with lower-degree polynomials to mitigate overfitting and ensure that the derived rheological parameters reflect material behavior rather than noise (Trefethen, 2013).

2.3. Matching creep curves using an improved method

This section presents an analysis of experimental results for the creep behavior under torsion of a composite material PVP (Polyvinylpyrrolidone). The material under torsional deformation was carried out earlier, using an "Instron-115" press. Continuous recording of the torsion angle variation was performed with the aid of electrotensometers. At that stage, only statistical processing of the obtained data and the preparation of corresponding

tables were conducted. In the present work, theoretical processing of these data was done, and the rheological parameters of the material (A, α, β) were determined.

The measuring instrument (indicator) is a micrometer with a measurement accuracy of Δh = 10 μm (see Figure 3). The twist angle is determined by the vertical displacement of the end of the rod attached to the specimen. This displacement results from the rotation of the rod together with the specimen during torsion. During measurement, after calibrating the instrument to 0 μm, the displacement values recorded under the minimum load exceed $h > 80\mu m$, in which case the relative measurement error of the instrument, $\Delta h / h$, does not exceed 10–11%. At higher loads, this relative error becomes even smaller.

The dimensions of the test specimen were chosen so that the influence of the clamps (boundary effects) would not affect the stress state of the working section of the specimen. To ensure reliable measurement values, it was necessary to establish a uniform stress state in the working section. The gauge length of the specimen did not exceed 5/6 of its total length (Dumbadze, 2015).

The test process was carried out in an environment where the following conditions were maintained: $T = 20° \pm 2$ ℃, humidity $W = 65\% \pm 5\%$;

Under conditions of a constant loading rate, short-term tests were conducted at M_z = 0.1 M_{tor}; 0.2 M_{tor}; 0.3 M_{tor}; 0.4 M_{tor}; 0.5 M_{tor}, where M_{tor} is the torsional load at which the specimen loses stability during short-term testing.

The specimens of different aging times were selected: $\tau = 1$ month, $\tau = 1$ year, and $\tau = 10$ years. Based on the obtained data, the improved method was used to determine the material's rheological parameters and the corresponding correction coefficients.

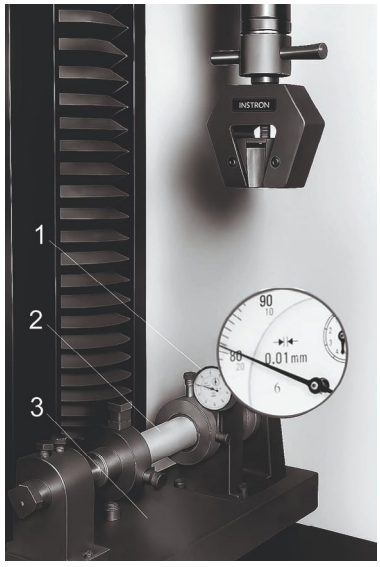

Figure 3. Experimental setup for torsional testing of the specimen: 1 – measuring indicator, 2 – test specimen, 3 – test device (source: Dumbadze, 2015)

The results of the experimental testing are summarized in Table 1, while the visual representations of the creep curves are shown in Figure 4.

The analysis is based on a cylindrical sample made of PVP material, characterized by the following parameters (Dumbadze, 2015):

- Outer diameter, $D = 40$ mm;
- Inner diameter, $d = 34$ mm;
- Length of the working section, $l = 180$ mm;
- Applied constant torque, $M_{tor} = 550$ kgf·cm;
- Polar moment of inertia of the cross-section $I_P = \frac{\pi D^4}{32}\left(1 - \left(\frac{d}{D}\right)^4\right)$.

For each load level, not fewer than three specimens were tested. After direct testing, the specimens were unloaded, and reverse creep behavior was observed. Based on the values $\varphi_n(t_m)$ obtained at each time t_m, the average creep strain values were calculated as: $\overline{\varphi}_n(t) = \frac{1}{n}\sum_{i=1}^{n}\varphi_i(t)$. The obtained data are presented in Table 1. The same source (Dumbadze, 2015) also provides statistical processing of the data, including the standard deviation and coefficient of variation (see Table 2).

It should be noted that information regarding the performance of fractographic analysis during the testing of the material is not provided in the referenced source, which has been conducted in the mentioned reference (Murataoglu & Bodugoz-Senturk, 2010).

Verification of the variation of these parameters is a technically challenging task, since after each change of a single parameter it is necessary to recalculate the points of the function graph, which requires significant time and resources. Understanding the variation of the influence-function parameters and evaluating the stability of the corresponding solutions can be accomplished using the data presented in the appendix of Dumbadze (2015), which provides tabulated values of the integrals containing the influence function together with graphs illustrating parameter variations. These graphs show that changes in the $K(t-\tau)$ (3) parameters (A, α, β) do not appreciably alter their graphical profiles, thereby indicating the stability of the solutions. Unfortunately, direct analytical application of the function is not feasible; therefore, the method of graph fitting was initially proposed, and subsequently the fitting method in terms of polynomial approximation was introduced and improved. Nevertheless, after fitting, it becomes possible to calculate the effective parameters of the function with relatively high accuracy. $A_{eff} = A(1.084)^{\alpha} = 0.0221$; $\alpha_{eff} = \alpha = 0.025$; $\beta_{eff} = 1.084\beta = 0.0542$.

The analysis of the presented graphs reveals distinct triplets that correspond to the test results of the material samples of three different ages, produced according to manufacturing date, under the same magnitude of torsional load. Each such triplet exhibits similarity, implying that if the analytical form of one curve (the base

Table 1. Creep deformations under torsion (PVP.*T* = 20 °C, *W* = 70%) (source: Dumbadze, 2015)

t Hours	M_z = 0.1 M_{tor}, kgf·cm			M_z = 0.2 M_{tor}, kgf·cm		
	τ = 10 Years	τ = 1 Year	τ = 1 Month	τ = 10 Years	τ = 1 Year	τ = 1 Month
0	0.0020	0.0024	0.0033	0.0033	0.0044	0.0055
5	0.0055	0.0072	0.0092	0.0127	0.0150	0.0188
10	0.0061	0.0083	0.0104	0.0144	0.0170	0.0211
20	0.0067	0.0090	0.0115	0.0162	0.0194	0.0240
50	0.0073	0.0094	0.0118	0.0171	0.0208	0.0250
100	0.0074	0.0096	0.0120	0.0177	0.0217	0.0269
150	0.0075	0.0096	0.0120	0.0179	0.0219	0.0271
	M_z = 0.3 M_{tor}, kgf·cm			M_z = 0.4 M_{tor}, kgf·cm		
0	0.0065	0.0025	0.0100	0.0100	0.0130	0.0160
5	0.0243	0.0277	0.0330	0.0398	0.0476	0.0600
10	00277	0.0315	0.0366	0.0430	0.0520	0.0680
50	0.0330	0.0343	0.0446	0.0570	0.0660	0.0830
80	0.0340	0.0396	0.0459	0.0598	0.0700	0.0860
100	0.0343	0.0405	0.0460	0.0609	0.0720	0.0860
150	0.0349	0.0410	0.0465	0.0614	0.0740	0.0870

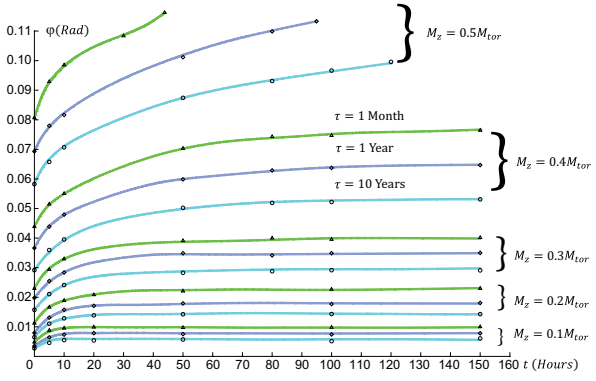

Figure 4. Time-dependent variation of the twist angle under torsional deformation (creep curves)

curve) is known, the others can be obtained by multiplying the base curve by the similarity coefficients. It should be noted that curves corresponding to different load magnitudes differ significantly, and it would be inappropriate to discuss their similarity. Additionally, it is important to highlight that when the applied torsional moment exceeds M_z > 0.4 M_{tor}, the material rapidly loses stability, which must be carefully considered during the subsequent design and manufacture of structural components made from this material, particularly regarding their strength and stability characteristics.

Table 2 presents the mean values of the twist angle $\bar{\varphi}$ obtained under the smallest applied load on the specimen, along with their standard deviations S_φ. The smallest load was selected based on the consideration that measurements at this level must be taken with particular care, as

Table 2. Average values $\bar{\varphi}$ and standard deviation S_φ of the twist angle under a load of M_z = 0.1 M_{tor} (source: Dumbadze, 2015)

M_z = 0.1 M_{tor}, kgf·cm						
τ = 1 Month			τ = 1 Year		τ = 10 Years	
t Hours	$\bar{\varphi}$ Degree	S_φ Degree	$\bar{\varphi}$ Degree	S_φ Degree	$\bar{\varphi}$ Degree	S_φ Degree
5	0.300	0.0046 (1.50%)	0.252	0.0040 (1.60%)	0.220	0.0044 (2.00%)
10	0.335	0.0052 (1.55%)	0.290	0.0048 (1.66%)	0.245	0.0051 (2.10%)
20	0.370	0.0057 (1.55%)	0.325	0.0053 (1.66%)	0.275	0.0057 (2.10%)
50	0.410	0.0063 (1.50%)	0.360	0.0060 (1.69%)	0.295	0.0062 (2.10%)
100	0.418	0.0066 (1.58%)	0.368	0.0062 (1.70%)	0.312	0.0071 (2.30%)
150	0.420	0.0067 (1.60%)	0.370	0.0063 (1.70%)	0.316	0.0073 (2.31%)

there is a high risk of obtaining significant measurement errors.

To establish the analytical form of the creep curves describing the material's torsional creep behavior, a base curve must be selected for each triplet, its corresponding analytical function parameters $(A, \alpha \text{ and } \beta)$ determined, and similarity coefficients calculated for the remaining two curves.

As an example, data corresponding to the torsional load M_z = 0.2 M_{tor} were selected. The curve for the sample aged $\tau = 1$ year was chosen as the base curve. According to Equation (8), it is necessary to calculate the twist angle intensity $\theta(t)$, which for the experimental curves can be easily determined by dividing the recorded twist angle values presented in Table 1 by the specimen length, according to Equation (4). By applying logarithmic transformations to Equation (8), the following relationship is obtained:

$$\ln\left[\theta_{\exp}\left(t_{\exp}\right)\right] = \ln\left(\frac{M_z}{GI_P}\right) + \ln\left[1 + \int_0^{t_{th}} K\left(t_{th} - \tau\right) d\tau\right] = \ln\left(\frac{M_z}{GI_P}\right) + \ln\left[f_{th}\left(t_{th}\right)\right], \quad (15)$$

where the notation is introduced for the theoretical curve

$$f_{th}\left(t_{th}\right) = 1 + \int_0^{t_{th}} K\left(t_{th} - \tau\right) d\tau\,. \quad (16)$$

In Equation (14), the theoretical and experimental functions are separated. The curve-fitting method involves maximizing the coincidence of the curves described by these functions. In the present case, the goal is to fit the curves described by $\ln\left[\theta_{exp}\left(t_{exp}\right)\right]$ $\ln\left[f_{th}\left(t_{th}\right)\right]$ with a constant accuracy coefficient, which will be determined later. For this specific case, the theoretical curve was selected both visually and by establishing simple mathematical proportional relationships for several points on the graph. Within the time interval from 5 to 150 hours, the best fit was obtained for the theoretical curve defined by the parameters: A = 0.02205, α = 0.025 and β = 0.05 (Dumbadze, 2015). The corresponding experimental and theoretical data are presented in Table 3.

As seen from the Table 3, the experimental data at the initial moment $t = 0$ are unreliable, while within the time interval from 5 to 150 hours, proportionality is maintained to a high degree. For more precise determination of the shifts (correction coefficients) during the fitting of the theoretical and experimental curves, an improved method was applied (Abesadze & Kopaliani, 2024). According to Equation (11), the experimental curve was approximated by the 4th-degree polynomial $P_4\left(\ln t_{exp}\right)$ using the least squares method, while the theoretical curve was approximated by the 7th-degree polynomial $P_7\left(\ln t_{th}\right)$ over the time interval $t_{th} = 1 - 300$ hours (the boundaries extend beyond the considered time interval). The polynomial coefficients were determined by solving the system of equations derived from the condition of coincidence between the theoretical function and the polynomial at 8 preselected points. Subsequently, the expression given by Equation (12) was constructed, and the system of equations defining the minimization of the sum (13) was solved. The calculations were performed using the computer algebra system Maple.

As a result, the correction coefficients for curve fitting, which establish the relationship between the theoretical and experimental functions and are expressed by the dependence in Equation (10), were obtained as follows:

$$a = 132.734 \text{ and } k = 1.084\,. \quad (17)$$

As a result, the expression for the torsion angle intensity defined by Equation (8) takes the form:

$$\theta_{\tau=1year}\left(t\right) = 0.0075\left[1 + \int_0^{1.084t} K\left(1.084t - \tau\right) d\tau\right]. \quad (18)$$

From Equation (8) it also follows that the coefficient preceding the function $f_{th}(t)$, according to equation (18), is $\frac{M_z}{GI_P} = 0.0075$, from which, considering the shear modulus of the given composite material, the torsional load, and the geometry of the tested specimen, it follows that:

$$G = \frac{0.2\ M_{tor}}{0.0075 \cdot I_P} = 1215.38\,. \quad (19)$$

Table 3. Experimental and theoretical results of creep under torsion for PVP material

t (Hours)	M_z = 0.2 M_{tor}, τ = 1 Year		$\alpha = 0.025;\ \beta = 0.05;\ A = 0.02205$	
	$\varphi_{\exp}(t)$	$\theta_{\exp}(t) = \frac{\varphi_{\exp}(t)}{l}$	$f_{th}(t) = 1 + \int_0^t K d\tau$	$\frac{f_{th}(t)}{\theta_{\exp}(t)}$
0	0.0044	0.0244	1.0	40.9836
5	0.0150	0.0833	10.8305	130.0180
10	0.0170	0.0944	12.4019	131.3760
20	0.0194	0.1078	14.0277	130.1271
50	0.0208	0.1156	15.5781	134.7586
100	0.0217	0.1206	15.9500	132.2554
150	0.0219	0.1217	15.9828	131.3295

From Equation (18), it is also seen that the value of the torsion angle intensity at time $t=0$ is $\theta(0)=0.0075$, while the torsion angle for the given specimen is $\varphi(0)=\theta(0)\cdot l=0.00135$ It is also possible to calculate the maximum shear stress induced in the specimen's cross-section using Equation (5):

$$\tau_{max}(0)=G\cdot R\cdot\theta(0)=\frac{G\cdot D\cdot\theta(0)}{2}=0.1823. \quad (20)$$

As noted, the curves corresponding to the load 0.2 M_{tor} for materials of different ages are similar. The base curve was taken as the torsional creep curve for the material aged $\tau=1$ year. For the other two, the torsional deformation behavior can be described as follows, considering Equation (18):

$$\theta_{\tau=1month}(t)=\lambda_1\cdot\theta_{\tau=1year}(t),$$
$$\theta_{\tau=10years}(t)=\lambda_2\cdot\theta_{\tau=1year}(t), \quad (21)$$

where λ_1 and λ_2 are the similarity coefficients, whose average values should be determined directly from the ratios of the coordinates of the corresponding torsional creep curve points (considering that the values at $t=0$ are not reliable). As well as the standard deviation values were also evaluated for the similarity coefficients according with reference (Montgomery & Runger, 2020; Moore et al., 2021). The results indicate that the maximum standard deviation of the average similarity coefficients is for $\Delta\lambda_1$ – 1.40% and for $\Delta\lambda_2$ – 1.72%. Based on the data presented in Table 1, the similarity coefficients are given as follows:

Using the proposed methodology, analogous calculations can be performed for different values of the applied torsional load M_z = 0.2 M_{tor}, as presented in Table 1. This process involves selecting a representative baseline creep curve, identifying the corresponding theoretical creep function $f(t_{th})$ within the framework of hereditary rheological theory, and determining its parameters $(A,\ \alpha$ and $\beta)$. The improved fitting method is then employed to accurately evaluate the correction coefficients that minimize the deviation between theoretical and experimental data. Subsequently, time-dependent functions of relevant quantities, such as twist intensity, maximum shear stress τ_{max}, and shear modulus G are derived in analytical form. Additionally, similarity coefficients are calculated to quantify the resemblance of creep behavior among materials of different aging durations under identical loading conditions.

During the research, it was observed that the deformation response of the material varies significantly under different types of mechanical loading, which is directly reflected in its rheological properties. For this reason, and to ensure clarity and focus, the study specifically analyzed one loading scenario in detail – torsional deformation at a stress level of M_z = 0.2 M_{tor}. Furthermore, it was found that material samples with different aging histories exhibit distinct deformation profiles under the same load; however, their respective creep curves demonstrate a high degree of similarity, as supported by the data in Table 4. Therefore, a specific baseline creep curve corresponding to a material $\tau=1$ year was selected. The rheological parameters were determined using the improved analytical method, including the computation of curve-fitting correction coefficients, the material's shear modulus G, and the maximum induced shear stress τ_{max}. For the other two samples with different aging times, similarity coefficients were evaluated relative to the selected baseline curve.

2.4. Comparison with other methods

The given problem has also been addressed within the framework of model theory, in particular through the use of five-element models applied both to elastic and plastic groups of polymers (Dumbadze, 2015; Abesadze, 2020). However, unlike the well-established tendencies observed in tensile deformation, where at low loads the properties of elastic-group polymers are expected to manifest, and at high loads the properties of plastic-group polymers the analysis of the present curves showed the opposite behavior. Furthermore, any variant of model theory, despite its mathematical simplicity and elegance, suffers from one major drawback: in the long-term perspective, the asymptotic behavior is always linear, whereas real experimental data do not conform to such a simplification. Therefore, the hereditary theory approach, despite its mathematical complexity, proves to be more adequate. The use of the proposed improved method within this framework allows for simplified calculations and enhanced accuracy.

Table 4. Similarity coefficients of the creep curves under torsion for PVP material

Time t (Hours)	M_z = 0.2 M_{tor}		M_z = 0.2 M_{tor}	
	$\lambda_1=\frac{\theta_{\tau=1month}(t)}{\theta_{\tau=1year}(t)}$	$\lambda_{1average}$	$\lambda_2=\frac{\theta_{\tau=10years}(t)}{\theta_{\tau=1year}(t)}$	$\lambda_{2average}$
5	1.2533	1.2351 ± 0.0173	0.8467	0.8307 ± 0.0143
10	1.2412		0.8471	
20	1.2371		0.8351	
50	1.2019		0.8221	
100	1.2396		0.8157	
150	1.2374		0.8174	

It is important to note in this context that the framework of Shapery's viscoelastic model, which is based on hereditary theory and the description of nonlinear viscoelastic effects, is inherently more suitable for isotropic polymeric materials. Its application to anisotropic composites requires additional validation and modification.

Accordingly, for future research it is desirable to broaden the scope of investigation to include a more diverse class of materials. Special emphasis should be placed on experimental studies of anisotropic composites under torsional deformation, in order to reveal general regularities and to define the practical limits of Shapery's model.

2.5. Compliance with standards under torsional loading and extension to other materials

Regarding the limitations of the method, it should be noted that it has already been tested on similar materials under relatively simpler tensile deformation and stress relaxation, where parameter identification was successfully achieved (Abesadze & Kelikhashvili, 2023). For other types of composite materials, different parameter combinations are to be expected, which must be addressed through individual studies. At the same time, the overall approach and methodology remain unchanged, ensuring the universality of its application.

In the conducted experiment, the standard ASTM D638-14 and ISO 527-1:1993 were applied (ASTM International, 2014; International Organization for Standardization, 1993). This normative document defines the load ranges, testing conditions, and permissible limits, which are essential to ensure the objectivity and reliability of the results.

3. Conclusions

The determination of rheological characteristics of composite materials under torsional deformation remains a significant challenge in both theoretical research and engineering practice. In the presented study, the team of authors successfully developed an improved method based on the analytical fitting of theoretical and experimental curves, employing an approach similar to the method of least squares. As a result, the rheological parameters of the material during the creep process are determined with high accuracy. The research integrates theoretical modeling and experimental data analysis, thereby ensuring the reliability and applicability of the results.

The main novelty of the study lies in the fact that the curve fitting is performed not based on visual assessment (as is common practice), but rather quantitatively, through the minimization of a specific mathematical criterion. This significantly reduces errors caused by human factors and enhances the precision of the analysis. The results give opportunity to design lightweight, high-strength composite parts for torsional loads, allowing engineers to refine safety factors and reduce structural weight without compromising performance.

In this study, the rheological parameters (A, α, and β) of the composite material PVP (Polyvinylpyrrolidone) were determined using the improved method; polynomial dependencies were established for the representation of theoretical curves; the material's shear modulus G and correction coefficients for curve fitting were calculated; similarity coefficients were determined for torsional creep curves of samples of different material aging under the same loading conditions. A refined methodology was developed, providing a basis for conducting similar rheological studies on other materials.

The practical significance of the research is that the proposed analytical approach can be applied in rheological analysis where high data accuracy is essential – for example, in the fields of aviation, mechanical engineering, and materials science. Notably, the developed method enables the prediction of long-term material behavior under specific loading conditions. This facilitates optimal material selection, informed structural design decisions, and accurate determination of safety margins. The method is also adaptable for the analysis of other types of deformation, offering opportunities for expanding the scope of the research.

One of the key contributions of this study to the aviation field is its direct relevance to the long-term structural reliability of aircraft. Composite materials, widely used in fuselage panels, wing structures, propeller blades, and rotor systems, are continuously subjected to complex combinations of torsional, tensile, and bending loads during flight. Over time, creep deformation can accumulate even under normal operating stresses, potentially resulting in residual strain and the gradual degradation of structural integrity. The improved curve-fitting method developed in this study enables precise modeling of these time-dependent effects, providing engineers with predictive tools to assess the lifespan and performance degradation of critical components.

Consequently, the presented approach contributes to enhancing flight safety, optimizing maintenance intervals, and improving the efficiency and sustainability of next-generation aircraft structures.

The authors' contribution to the research is evident in their active participation in both the development of the theoretical model and the processing and interpretation of data. The mathematical analysis methods, computational algorithms, and modeling framework they employed demonstrate a high level of execution, with outcomes that may be widely adopted in industrial practice in the future.

Future research directions include applying the proposed method to various types of loading conditions, both simple and combined; expanding the database of high-precision rheological parameters through additional experiments and digital simulations; and adapting the method and developing algorithms for integration into modern simulation software.

Acknowledgements

This work was supported by Shota Rustaveli National Science Foundation of Georgia (SRNSFG) [YS-23- 796, A New Method for Calculating Composite Spatial Constructions, Algorithm and Software].

Disclosure statement

The authors declare that there are no conflicts of interest related to this study. No financial support or benefits have influenced the research outcomes.

References

Abesadze, B. (2019). *Sapreni aparatebis kompozituri shemonakerebis simtkitzeze angarishis metodebis shedarebiti analizi* [Comparative analysis of methods for stress calculation for composite thin-wall spaced constructions] [Doctoral dissertation, Georgian Aviation University]. Georgian Aviation University Repository. https://iverieli.nplg.gov.ge/bitstream/1234/314597/1/Disertacia.pdf

Abesadze, B., & Kopaliani, S. (2024). Characterization of creep process in composite materials using an updated method within the framework of inheritance theory. *International Journal of Mechanical and Production Engineering*, *12*(11), 42–46. https://www.iraj.in/journal/journal_file/journal_pdf/2-1042-174221024342-46.pdf

Abesadze, B., & Kelikhashvili, V. (2023). An improved method for determining the parameters of the composite material rheological functions within the framework of the nonlinear theory of deformation. *Scientific-Technical Journal*, *Building*, *3*(67), 46–50. https://doi.org/10.36073/1512-3936

Abesadze, B. (2020). The pure bending task in case of composite rod based on four-element model. *Transactions of VSB – Technical University of Ostrava Civil Engineering Series*, *20*(1), 1–4.

Amir, A. L., Ishak, M. R., Yidris, N., Mohd Zuhri, M. Y., Asyraf, M. R. M., Razman, M. R., & Ramli, Z. (2024). Full-scale evaluation of creep coefficients and viscoelastic moduli in honeycomb sandwich pultruded GFRP composite cross-arms: Experimental and numerical study. *Results in Engineering*, *21*, Article 101850. https://doi.org/10.1016/j.rineng.2024.101850

ASTM International. (2014). *Standard test method for tensile properties of plastics* (ASTM D638-14). ASTM International.

Barbero, E. J. (2018). *Introduction to composite materials design* (2nd ed.). CRC Press.

Beer, F. P., Johnston, E. R., DeWolf, J. T., & Mazurek, D. F. (2015). *Mechanics of materials* (7th ed.). McGraw-Hill Education.

Draper, N. R., & Smith, H. (1998). *Applied regression analysis* (3rd ed.). Wiley. https://doi.org/10.1002/9781118625590

Dumbadze, A. (2015). *Kompozituri tanis mekanika* [Mechanics of composite body]. Georgian Aviation University Press. (in Georgian)

Epperson, J. F. (2013). *An introduction to numerical methods and analysis* (2nd ed.). Wiley.

Ferry, J. D. (2018). *Viscoelastic properties of polymers* (3rd ed.). Wiley.

Findley, W. N., Lai, J. S., & Onaran, K. (1976). *Creep and relaxation of nonlinear viscoelastic materials*. Dover Publications.

Gibson, R. F. (2016). *Principles of composite material mechanics* (4th ed.). CRC Press. https://doi.org/10.1201/b19626

International Organization for Standardization. (1993). *Plastics – Determination of tensile properties – Part 1*: *General principles* (ISO 527-1:1993). ISO.

Lakes, R. S. (2009). *Viscoelastic materials*. Cambridge University Press. https://doi.org/10.1017/CBO9780511626722

Montgomery, D. C., & Runger, G. C. (2020). *Applied statistics and probability for engineers* (7th ed.). Wiley.

Moore, D. S., McCabe, G. P., Craig, B. A., & Alwan, L. C. (2021). Introduction to the practice of statistics (10th ed.). W. H. Freeman.

Murataoglu, O. K., & Bodugoz-Senturk, H. (Inventors). (2010, August 19). *PVA hydrogels having improved creep resistance, lubricity, and toughness* (U.S. Patent Application No. US20100210752A1). U.S. Patent and Trademark Office.

Nijssen, R. P. L. (2015). *Composite materials*: *An introduction* (1st English ed., Rens Horn trans.). Inholland University of Applied Sciences. https://compositesnl.nl/wp-content/uploads/2019/10/Composites-an-introduction-1st-edition-EN.pdf

Trefethen, L. N. (2013). *Approximation theory and approximation practice*. SIAM.

Ward, I. M., & Sweeney, J. (2012). *Mechanical properties of solid polymers*. Wiley. https://doi.org/10.1002/9781119967125